2010

Kv4.2 channels tagged in the S1-S2 loop for alpha-bungarotoxin binding provide a new tool for studies of channel expression and localization

Leonard Moise
University of Rhode Island, lmoise@uri.edu

Jing Liu

See next page for additional authors

Citation/Publisher Attribution

Leonard Moise, Jing Liu, Evgeny Pryazhnikov, Leonard Khiroug, AndreasJeromin & Edward Hawrot (2010) Kv4.2 channels tagged in the S1-S2 loop for alpha-bungarotoxinbinding provide a new tool for studies of channel expression and localization, Channels, 4:2,115-123, DOI: 10.4161/chan.4.2.10878
Available at: https://doi.org/10.4161/chan.4.2.10878

Channels

ISSN: 1933-6950 (Print) 1933-6969 (Online) Journal homepage: https://www.tandfonline.com/loi/kchl20

$K_V4.2$ channels tagged in the S1-S2 loop for alpha-bungarotoxin binding provide a new tool for studies of channel expression and localization

Leonard Moise, Jing Liu, Evgeny Pryazhnikov, Leonard Khiroug, Andreas Jeromin & Edward Hawrot

To cite this article: Leonard Moise, Jing Liu, Evgeny Pryazhnikov, Leonard Khiroug, Andreas Jeromin & Edward Hawrot (2010) $K_V4.2$ channels tagged in the S1-S2 loop for alpha-bungarotoxin binding provide a new tool for studies of channel expression and localization, Channels, 4:2, 115-123, DOI: 10.4161/chan.4.2.10878

To link to this article: https://doi.org/10.4161/chan.4.2.10878

RESEARCH PAPER

Channels 4:2, 115-123; March/April 2010; © 2010 Landes Bioscience

K_V4.2 channels tagged in the S1-S2 loop for alpha-bungarotoxin binding provide a new tool for studies of channel expression and localization

Leonard Moise,[1,2,†] Jing Liu,[1,†] Evgeny Pryazhnikov,[3] Leonard Khiroug,[3] Andreas Jeromin[4] and Edward Hawrot[1,*]

[1]Department of Molecular Pharmacology, Physiology and Biotechnology; Brown University; Providence, RI USA; [2]EpiVax, Inc.; Providence, RI USA; and Department of Cell and Molecular Biology; University of Rhode Island; Providence, RI USA; [3]Neuroscience Center; University of Helsinki; Helsinki, Finland; [4]Banyan Biomarkers; Alachua, FL USA

[†]These authors contributed equally to this work.

Key words: K_V4.2, S1-S2 loop, alpha-bungarotoxin, trafficking, ion channel, mutagenesis

Abbreviations: ACh, acetylcholine; Bgtx, α-bungarotoxin; EGFP, enhanced green fluorescent protein; GFP, green fluorescent protein; HAP, high affinity peptide; nAChRs, nicotinic acetylcholine receptors; Tα1, *torpedo* nAChR α1; TIRF, total internal reflection fluorescence

We report the first successful insertion of an engineered, high-affinity α-bungarotoxin (Bgtx) binding site into a voltage-gated ion channel, K_V4.2, using a short, intra-protein embedded sequence (GGWRYYESSLEPYPDGG), derived from a previously described mimotope peptide, HAP. A major benefit to this approach is the ability to live-image the distribution and fate of functional channels on the plasma membrane surface. The Bgtx binding sequence was introduced into the putative extracellular loop between the S1 and S2 transmembrane domains of K_V4.2. Following co-expression with KChIP3 in tsA201 cells, S1-S2 HAP-tagged channels express at levels comparable to wild-type K_V4.2, and their activation and inactivation kinetics are minimally altered under most conditions. Binding assays, as well as live staining of surface-expressed K_V4.2 channels with fluorescent-Bgtx, readily demonstrate specific binding of Bgtx to HAP-tagged K_V4.2 expressed on the surface of tsA201 cells. Similar live-imaging results were obtained with HAP-tagged K_V4.2 transfected into hippocampal neurons in primary culture suggesting applicability for future in vivo studies. Furthermore, the activation kinetics of S1-S2-tagged K_V4.2 channels are minimally affected by the binding of Bgtx, suggesting a limited role if any for the S1-S2 loop in voltage sensing or gating associated conformational changes. Successful functional insertion of the HAP sequence into the S1-S2 linker of K_V4.2 suggests that other related channels may similarly be amenable to this tagging strategy.

Introduction

K_V4.2 is a fast transient (A-type) voltage-gated potassium channel of the *Shal* subfamily that contributes to transient, voltage-dependent K^+ currents in the nervous system (A currents) and the heart (transient outward current).[1-4] The physiological functions of K_V4.2 depend not only on the regulation of biophysical channel properties but also on the fine-tuning of subcellular localization and of cell-surface abundance.[5] The processes that influence trafficking and surface distribution patterns of these channels, therefore will affect their ability to contribute to cellular functions. Thus, it is of great interest to understand the subcellular organization of these channels in order to fully understand their physiological roles, and hence it is important to develop the tools necessary to address these questions in living neurons.

The mechanisms that specify channel trafficking and distribution, unfortunately, are not well known due to lack of suitable high-affinity probes.[6] Current knowledge of the trafficking and distribution of K_V4.2 is based largely on studies using immunohistochemistry techniques, i.e., antibodies against channel subunit epitopes in fixed cells,[7-10] or recently, with recombinant K_V4.2-enhanced green fluorescent protein (EGFP) fusion or c-Myc-tagged K_V4.2 constructs in live cells where questions remain as to the detailed functionality of the recombinant constructs.[10-12] In addition, indirect channel tagging by labeling proteins that interact with K_V channels, has been used to study channel trafficking.[7,13,14] Even though these approaches have been widely used to study channel trafficking, there are severe limitations to these techniques. The issue of antibody specificity, insufficiently characterized commercial polyclonal antibodies in particular, has regained the attention of the neuroscience research community.[15,16] In addition, when using GFP fusion proteins or epitope inserts, it is important to establish how channel function is affected by the GFP fusion or epitope insert.

*Correspondence to: Edward Hawrot; Email: Edward_Hawrot@Brown.edu
Submitted: 06/22/09; Revised: 12/06/09; Accepted: 12/08/09
Previously published online: www.landesbioscience.com/journals/channels/article/10878

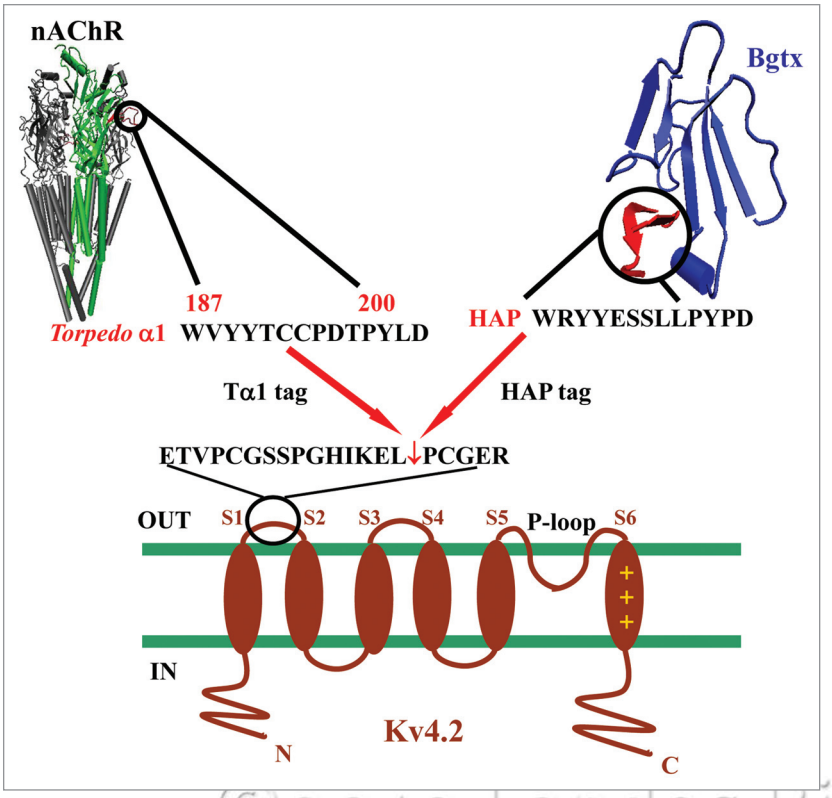

Figure 1. Schematic representation of the insertion of the HAP and Tα1 tag into the S1-S2 linker of K_V4.2. The diagrams depicting the structure of the neuronal nicotinic receptor (*left*) next to the structure of alpha-Bgtx (*right*) and the topology of K_V4.2 are shown. Two engineered sequences were inserted individually into the extracellular S1-S2 loop. One is derived from the principal Bgtx binding site on the *Torpedo* nAChR α1 subunit (Tα1) with sequence of WVYYTCCPDTPYLD. The other is from a high affinity peptide (HAP) sequence, WRYYESSLLPYPD, derived from a combinatorial phage-displayed library. These sequences were inserted into a location distant from the voltage sensor (S4) and ion selectivity filter (P loop) to minimize perturbation of the channel structure and function.

In the present study, we have generated and characterized a new chimeric construct, K_V4.2-HAP. HAP, a mimotope peptide of 13 amino acids in length, binds Bgtx with nanomolar affinity.[17,18] We introduced this Bgtx recognition sequence, bracketed at either end by two flexible Gly residues, into the extracellular S1-S2 loop of K_V4.2, presumably far from the critical gating sensor elements of the channel and from the N- and C-terminus (**Fig. 1**). Evidence from other K_V channel family members suggests that there is little S1 or S2 movement during voltage sensing and that movement of S1 or S2 does not play a significant role in gating.[19-21] This small extracellular tag sequence should limit potential perturbation of channel structure and function in comparison with a GFP tag. Bgtx is a small, soluble protein from the venom of the Taiwan banded krait *Bungarus multicinctus*. This unique high affinity ligand of muscle-type and α7 homo-oligomeric nAChRs (nicotinic acetylcholine receptors) has been instrumental in advancing many studies in structure, function and synaptic trafficking of nicotinic receptors for more than 3 decades.[22-25] In this study, we demonstrate that the chimeric construct of K_V4.2-HAP expresses as well as the wild-type K_V4.2 channel in mammalian cells, and that channel function is comparable to wild-type K_V4.2 channels even in the presence of Bgtx. By using fluorescent Bgtx, we were able to readily detect surface expression of K_V4.2 channels in living cells, including transfected primary neurons. The paradigm employed here, therefore, can be used as a general strategy for the design of chimeras for studying channel trafficking and distribution for other members of the K_V ion channel family.

Results

Insertion of bungarotoxin recognition sequences into the K_V4.2 S1-S2 loop. Two recognition sequences were designed and inserted individually into the extracellular S1-S2 loop of K_V4.2. One derived from the principal Bgtx binding site on the *Torpedo* nAChR α1 (Tα1) subunit and the other from a high affinity peptide (HAP) sequence derived from a combinatorial phage-displayed library.[17,26] These sequences were inserted into a location distant from the voltage sensor (S4) and ion selectivity filter to minimize perturbation of the channel structure and function (**Fig. 1**). Constructs were generated both with (i.e., K_V4.2-HAP-EGFP) and without (i.e., K_V4.2-HAP) cytoplasmic N-terminal EGFP-tags to facilitate visualization of K_V4.2-HAP. Studies of Tα1 chimera were limited by the low surface expression of this construct (e.g., see **Fig. 6A**), possibly because native disulfide formation between S1-S2 loop endogenous cysteines is disrupted by Tα1 cysteines.

Heterologously expressed K_V4.2-HAP constructs form functional channels. Following co-expression of K_V4.2-HAP with its auxiliary binding protein KChIP3 in tsA201 cells,[27] whole-cell recordings from transfected cells showed large, depolarization-activated, rapidly inactivating currents that resemble reported wild-type current in amplitude (**Fig. 2A**),[28,29] thus demonstrating functional expression of K_V4.2-HAP channels on the cell surface. Expression of K_V4.2-HAP constructs in transfected tsA201 cells was also validated by western blot analysis using an anti-K_V4.2 antibody (**Fig. 2B**).

Introduction of HAP tag sequence into S1-S2 is functionally silent. To determine the effect of HAP tag on K_V4.2 function, we compared the properties of K_V4.2-HAP to those of untagged K_V4.2 in tsA201 cells. In **Figure 3A**, we measured the time required for currents to reach peak amplitude in voltage steps from -30 mV to +50 mV. The rate of activation for K_V4.2-HAP was statistically different from wild-type K_V4.2 at more hyperpolarized potentials ranging from -30 mV to +10 mV ($p < 0.05$), but statistically indistinguishable from wild-type at more depolarized potentials ranging from +20 to +50 mV ($p > 0.05$). **Figure 3B** compares the peak conductance-voltage relation (G/G_{max}). The profiles of the voltage dependence of peak conductance/

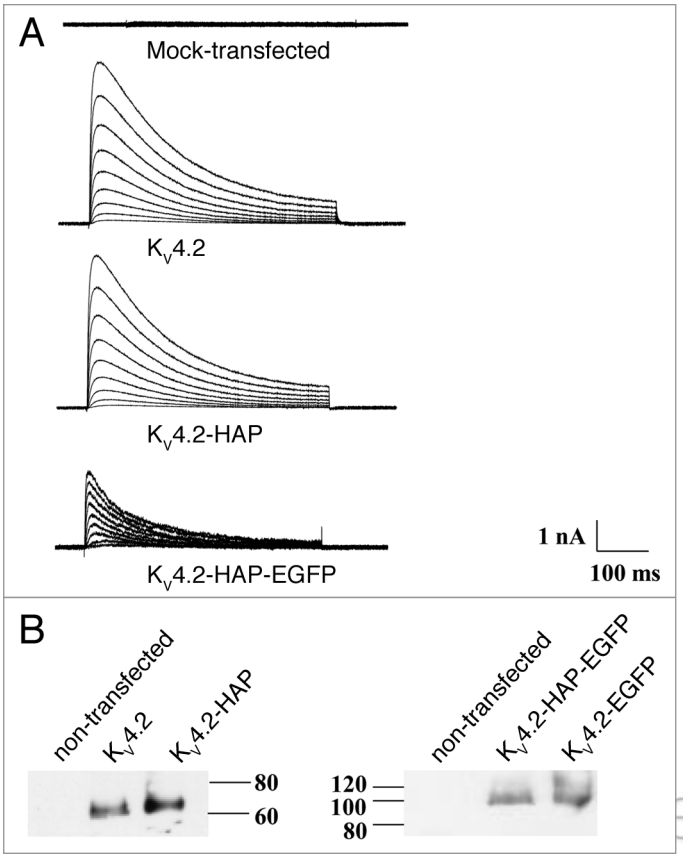

Figure 2. Heterologous expression of wild-type K_V4.2, HAP-tagged K_V4.2 (K_V4.2-HAP) and EGFP plus HAP-tagged K_V4.2 (K_V4.2-HAP-EGFP) in tsA201 cells. (A) K^+ currents in tsA201 cells were elicited by voltage clamp steps delivered at 10-mV increments from a holding potential of -80 mV to step depolarization from -30 mV to +50 mV (A, *inset*). Each voltage step was 600 ms long. Representative traces are from mock-transfected cells, or cells transfected with K_V4.2, K_V4.2-HAP or K_V4.2-EGFP-HAP as indicated. (B) Western blotting of K_V4.2 vs. K_V4.2-HAP and K_V4.2-HAP-EGFP vs. K_V4.2-EGFP. All constructs were detected with anti-K_V4.2 antibody.

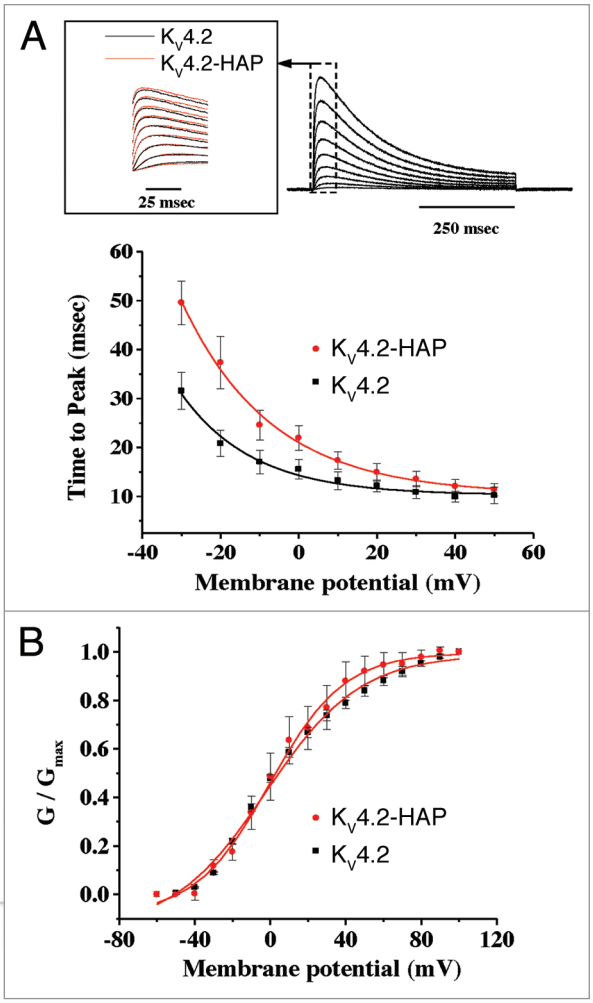

Figure 3. Activation kinetics for K_V4.2 (■) and K_V4.2-HAP (●). (A) Time to peak current analysis. Representative current traces of inactivation for K_V4.2 and K_V4.2-HAP are shown in Figure 1A. The upper panel shows detailed superimposed peak currents for K_V4.2 (black) and K_V4.2-HAP (red) in response to step membrane depolarization. Student's t test analysis showed that for voltage steps +20 mV to +50 mV the mean times to peak for K_V4.2 and K_V4.2-HAP were not significantly different ($p > 0.05$). In contrast, for the -30 to +10 mV range, the results are significantly different ($p < 0.05$). (B) Normalized peak conductance-voltage relations for K_V4.2 and K_V4.2-HAP. Normalized conductance (G/G_{max}, conductances at the indicated potential divided by G_{max}, the maximum conductance, at +50 mV) plotted as a function of voltage for the currents expressed by K_V4.2 and K_V4.2-HAP. Peak conductance (G) was calculated as $G = I_p/(V_m - V_{eq})$, where I_p, V_m and V_{eq} are the peak current, the test potential and the K^+ equilibrium potential, respectively. The continuous lines across the data points are the best-fits to Boltzmann functions. Values represent the Mean ± S.E.M of three to four cells. Normalized peak conductance-voltage relations for K_V4.2 and K_V4.2-HAP at all voltage steps are not significantly different by the Student's t test ($p > 0.05$).

activation of K_V4.2 and K_V4.2-HAP are not statistically different ($p > 0.05$). As shown in **Figure 4**, the overall profile of the voltage dependence of K_V4.2-HAP and wild type K_V4.2 inactivation are similar. Although significantly different at voltages of -30 mV, +30 mV, +40 mV and +50 mV ($p < 0.05$), at voltage steps ranging from -20 mV to +20 mV, the means of the inactivation time constants τ for K_V4.2 and K_V4.2-HAP are not significantly different ($p > 0.05$). The current decay fit very well with a single-exponential, and the rate of inactivation increased with strong depolarization. We also examined the recovery from inactivation (**Fig. 5**). Recovery was characterized using a typical two-pulse protocol where the time spent at the interpulse potential was varied to characterize the recovery time course. Statistical analysis shows the rates of recovery from inactivation for K_V4.2 and K_V4.2-HAP are not significantly different at all voltage steps ($p > 0.05$).

The functional analysis of K_V4.2-HAP shows that the insertion of HAP tag into the S1-S2 loop of K_V4.2 does not interfere with formation of functional channels. The expressed K_V4.2-HAP currents displayed fast inactivation and rapid inactivation with similar characteristics to K_V4.2. We conclude that insertion of the HAP sequence, within the S1-S2 linker, does not disrupt protein structure, subunit synthesis, or assembly.

Bgtx binds K_V4.2-HAP expressed in tsA201 cells. Specific binding of Bgtx to living cells was measured in a ^{125}I-Bgtx binding assay. Transfected tsA201 cells were incubated with radioactive

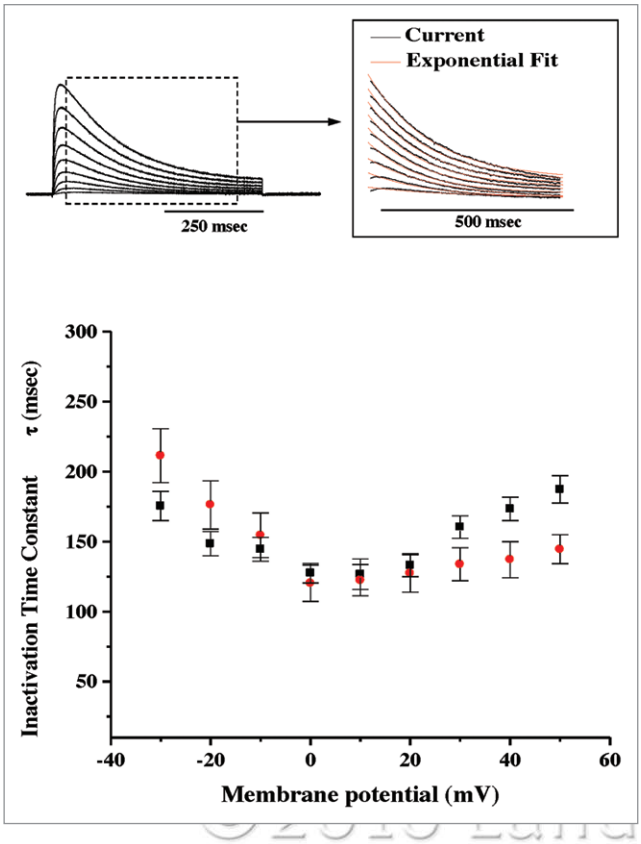

Figure 4. Inactivation time constants τ K_V4.2 (■) and τ K_V4.2-HAP (●). The upper panel shows inactivation kinetics of currents in response to step membrane depolarization. The time course of fast inactivation fits mono-exponentially. The continuous lines in red overlaid represent single exponential fits. Note that, the rate of inactivation increases with strong depolarization. Rate of inactivation decreased in the voltage range from -30 mV to 0 mV and increased from 0 mV to +50 mV. Values represent the Mean ± S.E.M of three to four cells. Student's t test analysis showed that the means of inactivation time constants τ for K_V4.2 and K_V4.2-HAP at voltage steps ranging from -20 mV to +20 mV are not significantly different ($p > 0.05$). In contrast, they are significantly different at voltage steps of -30 mV, +30 mV, +40 mV and +50 mV ($p < 0.05$).

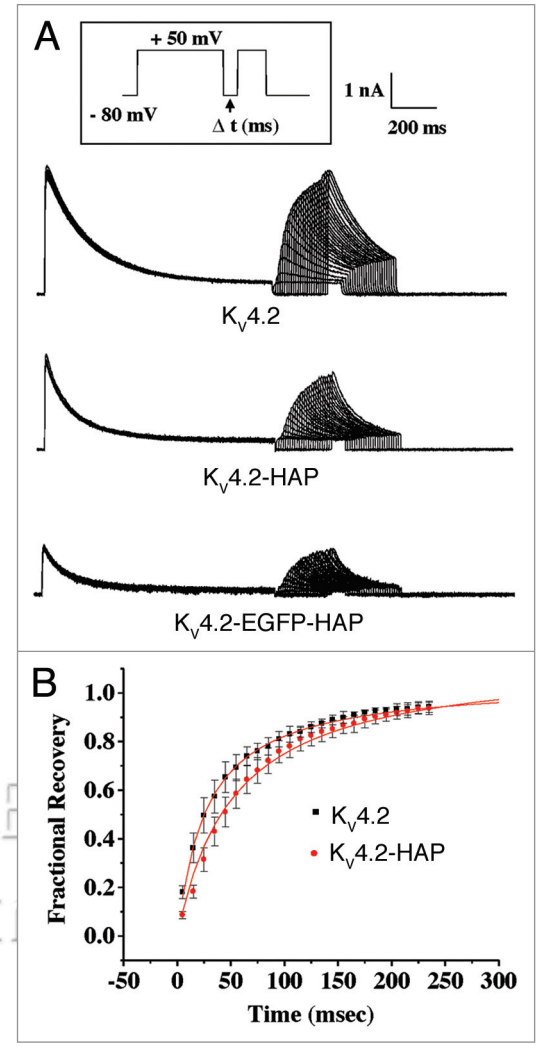

Figure 5. Rate of recovery from inactivation. (A) Representative current traces of the recovery from inactivation for K_V4.2, K_V4.2-HAP and K_V4.2-EGFP-HAP respectively are shown. A paired pulse protocol shown as an insert was applied to transfected tsA201 cells. Each cell was depolarized from -80 to +50 mV by two steps, varying the inter-step intervals (Δ*t*) from 5 ms to 245 ms in 10 ms increments. The membrane potential during the interval was also -80 mV. This set of paired pulses was applied once every 15 s. (B) The time course of recovery from inactivation is analyzed by normalizing the peak current amplitude of the second pulse to that of the first pulse and plotting as a function of inter-pulse duration. K_V4.2-HAP (●) recovers slightly more slowly from inactivation than wild-type K_V4.2 (■). Values represent the Mean ± S.E.M of data obtained from three to four cells. Applying the Student's t test, the rate of recovery from inactivation for K_V4.2-HAP is not significantly different ($p > 0.05$) from that of K_V4.2.

Bgtx, washed to remove unbound toxin, and then the cell associated radioactivity was determined (**Fig. 6A**). Specific Bgtx binding was observed for HAP-tagged K_V4.2 ($p < 0.05$), but not for Tα1-tagged channels ($p > 0.05$). Negative controls included untransfected cells and cells transfected with wild-type K_V4.2. Cells were transfected with muscle-type nAChR for a positive control. The binding results support the suitability of the HAP tag for tracking and visualizing surface expressed K_V4.2 channels in intact cells.

Bgtx binding affinity for K_V4.2-HAP was calculated by measuring association and dissociation with K_V4.2-HAP using the same ^{125}I-Bgtx binding protocol as that used for the basic binding assay. Association measurements over a 60 minute period yielded an apparent k_{on} value of 8.01×10^5 M^{-1} min^{-1}. An apparent dissociation rate k_{off} was measured by displacement of ^{125}I-Bgtx with excess unlabeled Bgtx and calculated as 7.4×10^{-3} min^{-1}. The ratio of k_{off} to k_{on} translates into an apparent equilibrium dissociation constant of 9.2×10^{-9} M.

Whole cell recordings were performed to measure the effect of Bgtx on K_V4.2-HAP channel function. The toxin had no significant effect on channel opening (**Fig. 6B**), suggesting that the bound toxin has limited functional effect when bound to the S1-S2 extracellular linker. Visualization of Bgtx bound to K_V4.2-HAP demonstrated the utility of HAP-tagged K_V4.2 for localization and membrane trafficking studies (**Fig. 7**). tsA201 cells transfected with either wild-type K_V4.2 or HAP-tagged K_V4.2,

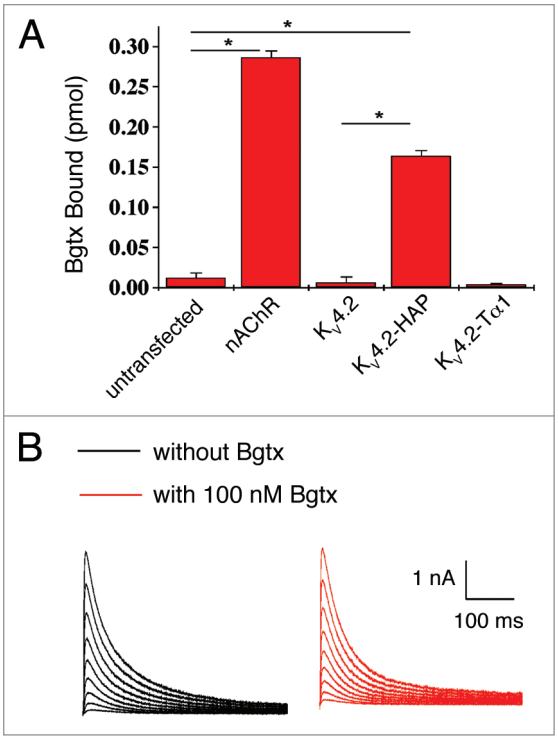

Figure 6. Binding of ^{125}I-Bgtx to K$_V$4.2-HAP and effect of Bgtx on K$_V$4.2-HAP currents. (A) Binding of ^{125}I-Bgtx to K$_V$4.2-HAP. tsA201 cells were incubated with ^{125}I for 2 h. Specific Bgtx binding was observed for K$_V$4.2-HAP as well as muscle-type nAChR ($p < 0.05$; denoted by asterisk,*), but not for K$_V$4.2 or K$_V$4.2-Tα1. Values represent the Mean ± S.E.M. The data shown are representative of three experiments. (B) Effect of Bgtx on K$_V$4.2-HAP currents. The current traces were recorded in the absence (black) or in the presence of 100 nM Bgtx (red). The presence of Bgtx had little effect on the activation of the channels.

and co-transfected with a GFP construct to identify expressing cells, were incubated with Alexa Fluor-Bgtx for 1 h at room temperature, washed and fixed. Fluorescent Bgtx was bound to cells expressing HAP-tagged K$_V$4.2 and was competed off in the presence of excess unlabeled Bgtx. No binding was observed with wild-type K$_V$4.2. Taken altogether, these results suggest that the insertion of the HAP sequence for Bgtx binding can offer a reliable method for tracking and isolating K$_V$4.2-HAP channels in living cells.

Bgtx binds K$_V$4.2-HAP and GluR2-HAP expressed in intact cultured hippocampal neurons. Although the HAP tag with Alexa Fluor-Bgtx enabled the visualization of K$_V$4.2 channels in living tsA201 cells, it was important to demonstrate a similar utility for this method in living neurons, to provide important validation that this tool could be used for the study of channel localization and mobility. Therefore, we studied the expression and subcellular distribution of HAP-tagged K$_V$4.2 in transfected rat hippocampal cultured neurons (**Fig. 8**). Cells were transfected with a construct encoding K$_V$4.2 with both a GFP fusion and the HAP insertion and treated with Bgtx (tagged with either Alexa Fluor or rhodamine). In order to avoid Bgtx binding to endogenous nicotinic ACh receptors, cells were preincubated with the nicotinic antagonist tubocurarine (2 μM) prior to application of Bgtx. To highlight perimembrane fluorescently-tagged molecules, total internal reflection fluorescence (TIRF) excitation mode was used. Images were obtained 18–36 hours after transfection using two fluorescence channels, green for GFP (excitation 488 nm, emission around 530 nm) and red for Bgtx-Alexa or Bgtx-rhodamine (excitation 532 nm, emission above 560 nm). Under this imaging configuration, the GFP image represents all recombinant K$_V$4.2 molecules independently of their membrane insertion, while the rhodamine-Bgtx image reveals membrane-inserted K$_V$4.2 molecules capable of binding extracellular Bgtx (**Fig. 8A**). We found that K$_V$4.2-HAP-GFP channels were distributed broadly along neuronal somata and dendrites (**Fig. 8A** and GFP clusters), but much fewer K$_V$4.2-HAP-GFP channels were located in the plasma membrane (**Fig. 8A**, rhodamine-Bgtx clusters). Analyses of cluster size yielded a significantly decreased value for clusters of membrane-inserted K$_V$4.2 channels, presumably due to aggregation of intracellular

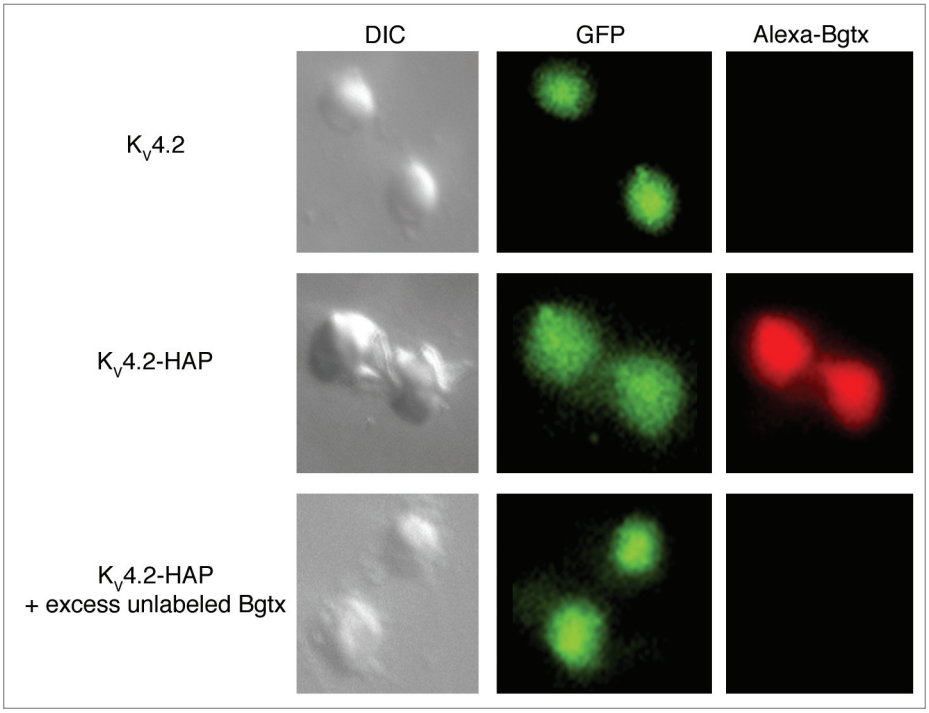

Figure 7. Alexa Fluor-Bgtx binds K$_V$4.2-HAP expressed in tsA201 cells. DIC, image of differential interference contrast; GFP, fluorescent image of GFP (detecting co-transfected GFP, green); Alexa Fluor-Bgtx, fluorescent image of Alexa Fluor-Bgtx (detecting K$_V$4.2-HAP, red). Wild-type K$_V$4.2 or HAP-tagged K$_V$4.2 was co-transfected with GFP in tsA201 cells. Fluorescent Bgtx bound HAP-tagged K$_V$4.2 and was competed off in the presence of excess unlabeled Bgtx. No fluorescent Bgtx binding was observed for wild-type K$_V$4.2.

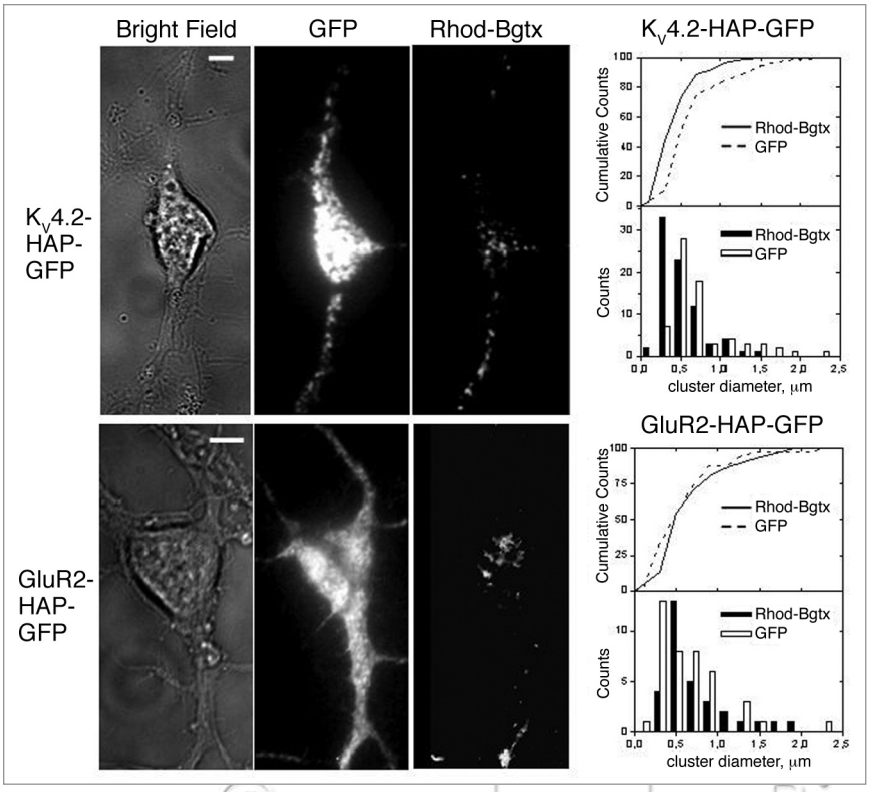

Figure 8. Rhodamine-Bgtx binds K_V4.2-HAP-GFP and GluR2-HAP-GFP expressed in primary rat hippocampal neurons. (A) A neuron transfected with K_V4.2-HAP-GFP. Bright Field, bright-field image of the neuron; GFP, fluorescence image of GFP (detecting all K_V4.2-HAP-GFP channels); Rhod.-Bgtx, fluorescence image of rhodamine-Bgtx (detecting membrane-inserted K_V4.2-HAP-GFP). (B) Cumulative curves and histograms of K_V4.2-HAP-GFP cluster size distribution obtained for green and red clusters (n = 6 cells). (C) A neuron transfected with GluR2-HAP-GFP. Bright Field, bright-field image of the neuron; GFP, fluorescence image of GFP (detecting both perimembrane and membrane-inserted GluR2-HAP-GFP channels); Rhod.-Bgtx, fluorescence image of rhodamine-Bgtx (detecting only membrane-inserted GluR2-HAP-GFP). (D) Cumulative curves and histograms of GluR2-HAP-GFP cluster size distribution obtained for green and red clusters (n = 3 cells). Scale bars: 5 μm.

K_V4.2 channels (**Fig. 8B**). Finally, we found that the cellular and surface distributions of K_V4.2-HAP-GFP expressed in hippocampal neurons appeared similar to those previously described for GluR2-HAP-GFP (**Fig. 8C**).[30]

Discussion

We have presented electrophysiological evidence that the functional parameters of K_V4.2-HAP channels closely resemble that of wild type K_V4.2. Furthermore, Bgtx binds K_V4.2-HAP specifically and with high affinity, and we were able to detect and image the tagged channels in live cells including in cultured neurons by using fluorescent Bgtx. Interestingly, although the HAP sequence introduces Bgtx binding, it produces no detectable pharmacological activity in the K_V4.2 background. Taken together, the successful introduction of the HAP binding sequence into the extracellular S1-S2 loop of K_V4.2 demonstrates that the HAP construct may serve as a flexible technique for labeling and visualization of ion channel trafficking in transfected primary neurons.

Bgtx as a high affinity ligand for muscle type and α7 nAChRs, has been extensively used more than 30 years to study the structure, function, distribution and trafficking of the receptor.[22-25] Recent studies using the Bgtx binding sequence have been very successful for ligand-gated ion channels,[24,25,30,31] as well as GPCRs,[32] but the use of this sequence in voltage-gated ion channels has not been previously reported. In most cases, including AMPA[30] and $GABA_A$ receptors,[33] as well as $GABA_B$ receptors,[32] the Bgtx binding sequence was placed at the N-terminus. Where the Bgtx binding site has been placed near the ion selectivity filter, as in the inositol 1,4,5-trisphosphate receptor (IP3R), Bgtx binding was observed to modulate IP3R single channel properties.[31] As binding of Bgtx has no observable effect on macroscopic K_V4.2 channel activation (**Fig. 6B**), we can conclude that with the HAP insertion site in K_V4.2 located in the extracellular S1-S2 loop, there is minimal if any interaction of bound Bgtx with the ion pore region. This in turn provides important structure-function information suggesting that the S1-S2 loop does not likely interact directly with residues contributing to the pore region.

Given that all currently commercially available antibodies against K_V4.2 label intracellularly located epitopes,[7-10] our extracellular HAP tag offers several advantages in that: (i) It facilitates labeling of surface expressed membrane protein in live cells, as reported here. (ii) The relatively small size of Bgtx (~8 kDa) and its flat shape as compared with globular antibodies (~150 kDa) should offer advantages in tissue penetration and accessibility. The corresponding Fab fragments and scFv chains of such antibodies, if available and as highly specific as the whole antibody, would still be larger in size and shape than Bgtx. (iii) The HAP tag offers advantages over conventional tags, such as HA and myc. Conventional tags are detected by antibodies, which raise concerns about the specificity and quality of the antibody reagent, especially because these reagents are often polyclonal and different laboratories use antibody reagents from different sources. Moreover, commercial polyclonal antibody production is often insufficiently controlled for quality or validated from batch to batch. These are significant concerns for the scientific community as it relies on dissemination of reliable and reproducible data. In comparison, Bgtx is highly specific for the HAP tag, as reported here and by others. Bungarotoxin is also in effect a "monoclonal" reagent of high homogeneity. It is a monogenic gene product from the snake *Bungarus multicinctus* that is purified from venom and has undergone rigorous characterization over 35 years in its native and labeled states by hundreds of independent laboratories. Because not all proteins can be tagged in easily accessible

regions for structural or functional reasons, a versatile tag detection system is advantageous. (iv) Moreover, a recent application of affinity purification with Bgtx-conjugated beads combined with mass spectrometry based proteomic analysis has identified an interactome for α7 nAChRs in the mouse brain.[34] Similar methodologies could be used to investigate K_V4.2 interactomes using HAP-tagged K_V4.2. (v) Fluorescent conjugates of Bgtx allow live staining of postsynaptic receptors in sympathetic ganglia from mice engineered with replacement of the native α3 nicotinic receptor subunit with one sensitive to Bgtx.[35] Live staining of the wild-type α3 nicotinic receptor subunit in any sympathetic or other neuronal preparation has not been possible with subunit-specific antibodies. (vi) Finally, quantum dots have increasingly been used for single-particle tracking studies of receptors and ion channels[36] by indirect detection of a peptide tag involving a biotinylated antibody and a streptavidin-quantum dot conjugate. The use of a Bgtx quantum dot conjugate for detection of K_V4.2 HAP ion channels and other membrane receptors offers the advantage of direct tag detection for higher-resolution single-molecule imaging.

K_V4.2 plays an important role in the modulation of neuronal function through formation of multi-protein complexes with signaling molecules and auxiliary proteins.[4,8,10,37] Although the use of tagged K_V4.2 binding proteins (i.e., KChIP, filamin or PSD95) has led to important insights about channel localization and trafficking,[7,38,39] those tags may indirectly affect K_V4.2 participation in functionally important multi-protein complexes. Thus, it is important to be able to visualize the tagged K_V4.2 channel itself.

The N- and C-termini of K_V4.2 channel are important for channel expression and interactions with channel signaling molecules and binding proteins.[4,13,37,40] Thus, modification of the N- and C-termini of the channel may complicate interpretation of the findings with these constructs. In particular, the GFP fusion protein, with its bulky N- or C-terminal tag could perturb important cellular functions. Therefore, it is significant that our engineered HAP insertion site is extracellular (S1-S2 loop) and far removed from the intracellular N- and C-termini. Our observation that application of Bgtx to HAP-tagged K_V4.2 has minimal effect on channel activation (**Fig. 6B**) further demonstrates that the S1-S2 loop can be sterically constrained with little apparent functional affect. Although the S1-S2 loop of K_V4.2 had previously been modified with an eight tandem repeat Myc tag insertion following Cys221, the effect of antibody binding on channel activity was not reported.[11] It is also of interest that the Tα1 sequence was poorly tolerated after insertion into the S1-S2 region of K_V4.2, while the HAP insertion into the same region, immediately after L219, was well tolerated. It is likely that the vicinal cysteines within the Tα1 sequence may interact with an extracellular disulfide involving the two endogenous cysteine residues in S1-S2 of K_V4.2. The HAP sequence, in contrast, lacks the native vicinal cysteines and would not be expected to alter the endogenous disulfide pattern of K_V4.2.

Finally, our findings offer the possibility that Bgtx recognition sequences can be similarly inserted into the extracellular domains of other K_V channels or, more broadly, into other membrane proteins for which appropriate probes are lacking. In cases in which high affinity Bgtx binding is conferred in the absence of pharmacological sensitivity, such constructs would be of considerable utility for studies of channel localization and trafficking given the variety of commercially available reporter group derivatives of Bgtx.[25]

Materials and Methods

Preparation of K_V4.2 mammalian expression constructs. HAP and Tα1 sequences were introduced into the K_V4.2 S1-S2 extracellular loop by oligonucleotide-directed mutagenesis using the Quikchange Mutagenesis kit (Stratagene). Mutant sequences were authenticated by DNA sequencing.

The introduced sequences are in bold italics and underlined.

S1-S2-loop-HAP chimera:

ETV PCG SSP GHI KEL ***GGW RYY ESS LEP YPD GG***P CGER

S1-S2-loop-Talpha1 chimera:

ETV PCG SSP GHI KEL ***GGW VYY TCC PDT PYL DGG*** PCG ER

S1-S2-loop: ETV PCG SSP GHI KEL PCG ER.

Culture and transfection of tsA201 cells. tsA201 cells are derived from a human embryonic kidney cell line containing a neomycin resistance gene and expressing T-antigen and were generously provided by Dr. William Green (University of Chicago, Chicago, IL). In our hands, the tsA201 cell line yielded 50% greater levels of cell surface Bgtx binding to *Torpedo* nAChR than the parental HEK 293 cells.[41] tsA201 cells were maintained at 37°C, 10% CO_2 in Dulbecco's modified essential medium (Invitrogen, Carlsbad, CA) supplemented with 10% fetal bovine serum, 10 μg/ml penicillin, and 10 units/ml streptomycin (all supplements obtained from Invitrogen).

Cells were transfected with K_V4.2 constructs, in combination with KChIP3 (K_V4.2:KChIP3 3:1), using Lipofectamine 2000 (Invitrogen). For non-EGFP-tagged proteins, GFP was co-expressed with the channel to assess transfection efficiency and to identify expressing cells for patch clamp experiments. Heterologous gene expression was driven off a CMV promoter on a pcDNA3.1 background.

For fluorescence imaging, tsA201 cells were seeded on poly-L-lysine-coated cover slips and stained following transfection, as described below. For electrophysiology experiments, cells were resuspended, washed and replated in a recording chamber 36–48 h after transfection. GFP-positive cells were patch clamped, as described below.

Preparation and transfection of primary rat hippocampal neurons. All studies were performed in full compliance with the standards of the University of Helsinki Institution Animal Care and Use Committee. Cultured neurons were prepared from embryonic day 18 rat hippocampi. Hippocampi were dissociated with Papain solution (10 U/mL). The cells were plated at a density of 3 x 10^4 cells per cm^2 on glass bottomed Petri dishes (MatTek) pre-treated with poly-L-lysine and laminin (1–2 μg/cm^2). Cultures were maintained in 5% CO_2/95% air atmosphere at 37°C in Neurobasal medium (Invitrogen, pH 7.4) supplemented with B27 (Invitrogen), 0.5 mM L-glutamine, 100 units/mL

penicillin and 100 μg/mL streptomycin. Medium was changed twice per week. Neurons were transfected after 7–10 days in vitro with K_V4.2-HAP-GFP construct using Lipofectamine 2000 (Invitrogen) according to the manufacturer's instructions. Cells were analyzed 18–36 hours after transfection.

Electrophysiology. Whole-cell patch clamp technique was used to assess the functional expression of K_V4.2, K_V4.2 HAP, and (EGFP-tagged) in transfected tsA201 cells. An Axopatch 200B amplifier (Axon Instruments, Foster City, CA) was used to record ionic currents with the whole cell voltage-clamp technique.[42] Current stimulus protocols and data collection were performed using pClamp 9.0 software (Axon Instruments, Foster City, CA). Pipettes were pulled on a multiple stage puller (Sutter Instruments, Novato, CA) from borosilicate tubing and polished to a resistance of 3–4 MΩ. Cells were bathed in standard extracellular solution containing (in mM): 140 NaCl, 5.4 KCl, 2.8 $CaCl_2$, 0.18 $MgCl_2$, 10 HEPES, 5.6 Glucose, 2 Glutamine (pH 7.4). The pipette solution contained (in mM): 140 KCl, 5 NaCl, 1 $MgCl_2$, 10 EGTA, 10 HEPES (pH 7.4). Leak-subtraction was performed before each recording. Series resistance (5–15 MΩ) was compensated (80–90%) manually and regularly monitored. Data were filtered at 5 kHz, sampled at 10 kHz and stored online. For the activation phase of K_V4.2-mediated currents the 10–90% rise time was determined. Conductance values (G) at a given test potential (V_m) were calculated from the measured peak amplitude (I) and the mean reversal potential for K_V4.2 ($V_{rev} \approx$ -40 mV; n = 4) using the equation $G = I/(V_m - V_{rev})$. The obtained data were further processed using Origin7.5 (Microcal Software, Inc., Northampton, MA). The voltage dependencies of activation and inactiyation were fitted with the Boltzmann function. Data are expressed as original traces and/or as mean ± S.E.M. Student's t test was used for statistical analysis. Probabilities of $p < 0.05$ were considered statistically significant. Co-transfected cells were identified by fluorescence microscopy using an inverted Axiovert 25 microscope (Carl Zeiss, Germany) equipped for fluorescence detection. All recordings were conducted at room temperature (22–25°C).

Binding experiments. Surface expression of tagged K_V4.2 channels was measured in a ^{125}I-Bgtx binding assay. ^{125}I-Labeled Bgtx (5 nM) was incubated in the presence or absence of unlabeled Bgtx with transfected cells in high-K Ringer's buffer for 2 h at room temperature. Following the incubation, cells were captured on Whatman GF/C filters (25 mm) and washed 4 times with 5 mL of high-K Ringer's buffer. Bound ^{125}I-Bgtx was measured in a γ counter. All measurements were done in triplicate, averaged and standard error calculated. Student's t test was used for pairwise comparisons with $p < 0.05$ considered statistically significant. Controls included cells not transfected and cells transfected with wild-type K_V4.2 and muscle-type nAChR. Specific Bgtx binding was calculated by subtraction of non-specific binding, as measured by ^{125}I-Bgtx binding in the presence of 2.5 μM unlabeled Bgtx, from total binding. For binding dissociation measurements, Bgtx was displaced by addition of 2.5 μM unlabeled Bgtx, following pre-incubation with ^{125}I-Bgtx to equilibrium over 2 h. Remaining bound toxin was measured over multiple points during a 60 minute period. Data were fit according to a two-component dissociation using:

$$y = y_0 + A_1 e^{xt1} + A_2 e^{xt2}$$

with the second exponential term negligible because of the rapid reduction in ^{125}I-Bgtx binding upon addition of unlabeled Bgtx. Bgtx binding association data collected over a 60 minute period were fit according to:

$$y = A_1 - A_2 e^{-k_{ob} x}$$

to calculate an observed k_{ob}, from which the apparent k_{on} was calculated according to:

$$k_{on} = \frac{k_{ob} - k_{off}}{[radioligand]}$$

Western blot. From tsA201 cells transfected with K_V4.2, K_V4.2-HAP and KChIP cDNAs, total cell lysates were prepared (lysis buffer: 150 mM NaCl, 50 mM Hepes pH 7.4, 0.5% Triton) and insoluble matter pelleted. Equal amounts of the supernatant were separated by 4–15% gradient SDS-PAGE following heat denaturation at 37°C for one hour in SDS-gel loading buffer. Separated proteins were transferred to nitrocellulose membranes. Following a blocking incubation (PBS; 0.05% Tween; 5% non-fat milk powder), K_V4.2-antibody (Alomone Labs) was diluted 1:200 and incubated at room temperature for two hours. After washing the membrane, horseradish-peroxidase-conjugated goat anti-rabbit IgG antibody (1:10,000) was incubated for 1 h. Enhanced chemiluminescence reagents were used for signal detection.

Fluorescence imaging. To assess K_V4.2-HAP protein expression in live tsA201 cells, cultures were mounted on glass slides and washed with PBS and incubated with Alexa Fluor-Bgtx for 1 h at room temperature. Cells were washed with PBS and fixed with 4% paraformaldehyde to stabilize the preparation for viewing. In all cases, fluorescent Bgtx binding was prevented by co-incubation with an excess of unlabeled Bgtx. Cells were imaged using a Zeiss Axiovert 200M Fluorescence Imaging microscope (Carl Zeiss, Inc.,) equipped with a Roper CoolSnap CF color camera and a Roper CoolSnap HQ monochrome camera (Roper Scientific, Inc.,) controlled by MetaMorph 6.0 software.

For TIRF imaging experiments on primary neurons, cell-containing MatTek dishes were transferred to the CellR imaging system (Olympus Europe, Hamburg, Germany). The system was equipped with an automated filter wheel for excitation filters and with 488 nm (20 mW) and 532 nm (50 mW) DPSS lasers (Melles Griot, CA, USA) for TIRF imaging. For improved recording stability, the microscope frame and all optical elements were maintained at 34°C using the temperature control incubator (Solent Scientific, Segensworth, UK). Images were collected with a CCD camera (Orca, Hamamatsu, Japan). In TIRF mode, fluorescent molecules are excited by the thin evanescent field formed above the glass substrate due to total internal reflection of the laser beam (attenuated to 5–10%). To block binding of tagged Bgtx to any endogenous nicotinic receptors, the transfected neurons were preincubated for at least 30 minutes with the nicotinic receptor antagonist tubocurarine

(2 μM) prior to incubation with 5 μg/ml rhodamine- or AlexaFluor-conjugated Bgtx to label the K_V4.2-HAP channels. Fluorescence of tagged Bgtx was excited at 532 nm and collected above 560 nm, and fluorescence of GFP was excited at 488 nm and collected between 515 and 545 nm.

Acknowledgements

This work was done in partial fulfillment of the requirements for a Ph.D. degree from Brown University (to Jing Liu). This research was supported by Research Grant GM32629 (Edward Hawrot) from the National Institutes of Health. Leonard Khiroug and Evgeny Pryazhnikov are thankful to the Academy of Finland and Center for International Mobility (CIMO) of Finland for financial support.

References

1. Dixon JE, Shi W, Wang HS, McDonald C, Yu H, Wymore RS, et al. Role of the K_V4.3 K^+ channel in ventricular muscle. A molecular correlate for the transient outward current. Circ Res 1996; 79:659-68.
2. Fiset C, Clark RB, Shimoni Y, Giles WR. Shal-type channels contribute to the Ca^{2+}-independent transient outward K^+ current in rat ventricle. J Physiol 1997; 500:51-64.
3. Kaab S, Dixon J, Duc J, Ashen D, Nabauer M, Beuckelmann DJ, et al. Molecular basis of transient outward potassium current downregulation in human heart failure: a decrease in K_V4.3 mRNA correlates with a reduction in current density. Circulation 1998; 98:1383-93.
4. Bahring R, Dannenberg J, Peters HC, Leicher T, Pongs O, Isbrandt D. Conserved K_V4 N-terminal domain critical for effects of K_V channel-interacting protein 2.2 on channel expression and gating. J Biol Chem 2001; 276:23888-94.
5. Heusser K, Schwappach B. Trafficking of potassium channels. Curr Opin Neurobiol 2005; 15:364-9.
6. MacKinnon R. Potassium channels. FEBS Lett 2003; 555:62-5.
7. Wong W, Newell EW, Jugloff DG, Jones OT, Schlichter LC. Cell surface targeting and clustering interactions between heterologously expressed PSD-95 and the Shal voltage-gated potassium channel, K_V4.2. J Biol Chem 2002; 277:20423-30.
8. Anderson AE, Adams JP, Qian Y, Cook RG, Pfaffinger PJ, Sweatt JD. K_V4.2 phosphorylation by cyclic AMP-dependent protein kinase. J Biol Chem 2000; 275:5337-46.
9. Takeuchi S, Takagishi Y, Yasui K, Murata Y, Toyama J, Kodama I. Voltage-gated K(+)Channel, K_V4.2, localizes predominantly to the transverse-axial tubular system of the rat myocyte. J Mol Cell Cardiol 2000; 32:1361-9.
10. Gardoni F, Mauceri D, Marcello E, Sala C, Di Luca M, Jeromin A. SAP97 directs the localization of K_V4.2 to spines in hippocampal neurons: regulation by CaMKII. J Biol Chem 2007; 282:28691-9.
11. Rivera JF, Ahmad S, Quick MW, Liman ER, Arnold DB. An evolutionarily conserved dileucine motif in Shal K^+ channels mediates dendritic targeting. Nat Neurosci 2003; 6:243-50.
12. Kunjilwar K, Strang C, DeRubeis D, Pfaffinger PJ. KChIP3 rescues the functional expression of Shal channel tetramerization mutants. J Biol Chem 2004; 279:54542-51.
13. Pourrier M, Herrera D, Caballero R, Schram G, Wang Z, Nattel S. The K_V4.2 N-terminal restores fast inactivation and confers KChIP2 modulatory effects on N-terminal-deleted K_V1.4 channels. Pflugers Arch 2004; 449:235-47.
14. Hasdemir B, Fitzgerald DJ, Prior IA, Tepikin AV, Burgoyne RD. Traffic of K_V4 K^+ channels mediated by KChIP1 is via a novel post-ER vesicular pathway. J Cell Biol 2005; 171:459-69.
15. Rhodes KJ, Trimmer JS. Antibodies as valuable neuroscience research tools versus reagents of mass distraction. J Neurosci 2006; 26:8017-20.
16. Moser N, Mechawar N, Jones I, Gochberg-Sarver A, Orr-Urtreger A, Plomann M, et al. Evaluating the suitability of nicotinic acetylcholine receptor antibodies for standard immunodetection procedures. J Neurochem 2007; 102:479-92.
17. Balass M, Katchalski-Katzir E, Fuchs S. The alpha-bungarotoxin binding site on the nicotinic acetylcholine receptor: analysis using a phage-epitope library. Proc Natl Acad Sci USA 1997; 94:6054-8.
18. Harel M, Kasher R, Nicolas A, Guss JM, Balass M, Fridkin M, et al. The binding site of acetylcholine receptor as visualized in the X-Ray structure of a complex between alpha-bungarotoxin and a mimotope peptide. Neuron 2001; 32:265-75.
19. Posson DJ, Selvin PR. Extent of voltage sensor movement during gating of shaker K^+ channels. Neuron 2008; 59:98-109.
20. Gandhi CS, Clark E, Loots E, Pralle A, Isacoff EY. The orientation and molecular movement of a k(+) channel voltage-sensing domain. Neuron 2003; 40:515-25.
21. Gonzalez C, Morera FJ, Rosenmann E, Alvarez O, Latorre R. S3b amino acid residues do not shuttle across the bilayer in voltage-dependent Shaker K^+ channels. Proc Natl Acad Sci USA 2005; 102:5020-5.
22. Fambrough DM, Hartzell HC. Acetylcholine receptors: number and distribution at neuromuscular junctions in rat diaphragm. Science 1972; 176:189-91.
23. Couturier S, Bertrand D, Matter JM, Hernandez MC, Bertrand S, Millar N, et al. A neuronal nicotinic acetylcholine receptor subunit (alpha7) is developmentally regulated and forms a homo-oligomeric channel blocked by alpha-BTX. Neuron 1990; 5:847-56.
24. Levandoski MM, Lin Y, Moise L, McLaughlin JT, Cooper E, Hawrot E. Chimeric analysis of a neuronal nicotinic acetylcholine receptor reveals amino acids conferring sensitivity to alpha-bungarotoxin. J Biol Chem 1999; 274:26113-9.
25. Sanders T, Hawrot E. A novel pharmatope tag inserted into the beta4 subunit confers allosteric modulation to neuronal nicotinic receptors. J Biol Chem 2004; 279:51460-5.
26. Kasher R, Balass M, Scherf T, Fridkin M, Fuchs S, Katchalski-Katzir E. Design and synthesis of peptides that bind alpha-bungarotoxin with high affinity. Chem Biol 2001; 8:147-55.
27. Rhodes KJ, Carroll KI, Sung MA, Doliveira LC, Monaghan MM, Burke SL, et al. KChIPs and K_V4 alpha subunits as integral components of A-type potassium channels in mammalian brain. J Neurosci 2004; 24:7903-15.
28. Hoffman DA, Magee JC, Colbert CM, Johnston D. K^+ channel regulation of signal propagation in dendrites of hippocampal pyramidal neurons. Nature 1997; 387:869-75.
29. Yeola SW, Snyders DJ. Electrophysiological and pharmacological correspondence between K_V4.2 current and rat cardiac transient outward current. Cardiovasc Res 1997; 33:540-7.
30. Sekine-Aizawa Y, Huganir RL. Imaging of receptor trafficking by using alpha-bungarotoxin-binding-site-tagged receptors. Proc Natl Acad Sci USA 2004; 101:17114-9.
31. Dellis O, Dedos SG, Tovey SC, Taufiq Ur R, Dubel SJ, Taylor CW. Ca^{2+} entry through plasma membrane IP3 receptors. Science 2006; 313:229-33.
32. Wilkins ME, Li X, Smart TG. Tracking cell surface $GABA_B$ receptors using an alpha—bungarotoxin-tag. J Biol Chem 2008.
33. Bogdanov Y, Michels G, Armstrong-Gold C, Haydon PG, Lindstrom J, Pangalos M, et al. Synaptic $GABA_A$ receptors are directly recruited from their extrasynaptic counterparts. EMBO J 2006; 25:4381-9.
34. Paulo J, Brucker W, Hawrot E. Proteomic analysis of an alpha7 nicotinic acetylcholine receptor interactome. J Proteome Res 2009; 8:1849-58.
35. Caffery PM, Krishnaswamy A, Sanders T, Liu J, Hartlaub H, Klysik J, et al. Engineering neuronal nicotinic acetylcholine receptors with functional sensitivity to α-bungarotoxin: a novel α3-knock-in mouse. Eur J Neurosci 2009; 30:2064-76.
36. Alcor D, Gouzer G, Triller A. Single-particle tracking methods for the study of membrane receptors dynamics. Eur J Neurosci 2009; 30:987-97.
37. Callsen B, Isbrandt D, Sauter K, Hartmann LS, Pongs O, Bahring R. Contribution of N- and C-terminal K_V4.2 channel domains to KChIP interaction. J Physiol 2005; 568:397-412.
38. Wang Z, Eldstrom JR, Jantzi J, Moore ED, Fedida D. Increased focal K_V4.2 channel expression at the plasma membrane is the result of actin depolymerization. Am J Physiol Heart Circ Physiol 2004; 286:749-59.
39. Petrecca K, Miller DM, Shrier A. Localization and enhanced current density of the K_V4.2 potassium channel by interaction with the actin-binding protein filamin. J Neurosci 2000; 20:8736-44.
40. Han W, Nattel S, Noguchi T, Shrier A. C-terminal domain of K_V4.2 and associated KChIP2 interactions regulate functional expression and gating of K_V4.2. J Biol Chem 2006; 281:27134-44.
41. Spura A, Russin TS, Freedman ND, Grant M, McLaughlin JT, Hawrot E. Probing the agonist domain of the nicotinic acetylcholine receptor by cysteine scanning mutagenesis reveals residues in proximity to the alpha-bungarotoxin binding site. Biochemistry 1999; 38:4912-21.
42. Hamill OP, Marty A, Neher E, Sakmann B, Sigworth FJ. Improved patch-clamp techniques for high-resolution current recording from cells and cell-free membrane patches. Pflugers Arch 1981; 391:85-100.